Accuracy and Resolution of Earth Radiation Budget Estimates

RICHARD N. GREEN

NASA Langley Research Center, Hampton, VA 23665

(Manuscript received 18 May 1982, in final form 1 December 1982)

ABSTRACT

A numerical filter inversion technique that reduces wide-angle satellite measurements to top-of-the-atmosphere radiant exitances has been proposed for the Earth Radiation Budget Experiment (ERBE). The matrix formulation of this technique is presented, and the design of the numerical filter is discussed. The filter is smoothed with a singular value decomposition. The inversion process is simulated by generating synthetic measurements from a 24 degree spherical harmonic radiation field derived from Nimbus 6 ERB data. The numerical filter is applied to these measurements after they are corrupted with instrument error. The results are curves of expected error versus resolution area.

1. Introduction

It is well established that the Earth's radiation budget can be measured from orbiting satellites with wide-angle radiometers. These observations are transformed by suitable data analysis techniques to estimate the radiant exitance field at the top of the atmosphere (TOA). Part of the estimation process is to establish the accuracy and resolution of these estimates. The accuracy of wide-angle inversion techniques has been the subject of several investigations (e.g., Green, 1980; King and Curran, 1980; Weaver and Green, 1980). Green (1981) has compared three different techniques and discusses the errors intrinsic to the techniques themselves. The question of resolution has been discussed by Smith and Green (1981), and Bess *et al.* (1981) for the deconvolution technique where resolution was related to the truncation of a spherical harmonic series representation of the radiation field.

The next major effort to measure the radiation budget is the Earth Radiation Budget Experiment (ERBE). It proposes to reduce the wide-angle satellite measurements to the top of the atmosphere with a numerical filter. This technique was first formulated by House and Jafolla (1980) and enhances the resolution of radiation field along the satellite groundtrack. The deconvolution technique (Smith and Green, 1981) enhances the radiation field in both latitude and longitude, but requires a global data set over a period of days. One of the ERBE requirements is an instantaneous estimate so that the diurnal variation can be modeled. This requirement of an instantaneous estimate restricts the enhancement to one dimension, or along the groundtrack. The purpose of this paper is to determine the accuracy and resolution of the Earth radiation budget as produced by the one-dimensional numerical filter technique.

The wide field-of-view measurement is the sum of all the radiation over a large area and, by its very nature, gives a smoothed representation of the true field. These measurements must be unsmoothed or enhanced to estimate the true field. The numerical filter accomplishes this by processing a sequence of measurements along the orbital track. The measurements are formulated in a matrix equation which is inverted to give the inversion weights for the numerical filter. The amount of data that is processed at one time is one of the design parameters which is examined in this paper.

The question of accuracy is best answered here by numerical simulation of the data gathering and estimation process. The orbital geometry has been defined and a typical longwave radiation field has been chosen which is taken as "truth." Synthetic measurements are calculated over this assumed radiation field and corrupted with random measurement errors. Applying the numerical filter to these synthetic measurements produces an estimate at the top of the atmosphere which is compared to the true radiation field to establish the accuracy. The approach taken is to form an estimator (numerical filter) of the radiant exitance and to establish its characteristics. One such characteristic is its ability to estimate the average radiant exitance over a circular area centered at the sub-satellite point. The size of the circle that produces an average radiant exitance that most closely matches the estimate is defined as the resolution. The difference between this average and the estimate is defined as the accuracy of the estimate. The variance

of this error leads to a statement of confidence on how well the radiant exitance can be estimated for small regions.

2. Formulation of numerical filter

The longwave measurement from a wide angle, flat plate radiometer at satellite altitude is given by

$$m(\Theta_s, \Phi_s, h; t) = \pi^{-1} \int_{\text{FOV}} M(\Theta, \Phi; t) R(\Theta, \Phi, \theta) \cos\alpha d\Omega, \quad (1)$$

where the measurement m is at a latitude Θ_s, longitude Φ_s, satellite altitude h, and time t; M is the radiant exitance at the top of the atmosphere, R the angular directional model for emitted radiance at zenith angle θ (Green, 1981), α the nadir angle, Ω solid angle, and the integration is over the field of view, FOV. Since the radiant exitance is defined at the top of the atmosphere, it is convenient to define h as the satellite altitude above the TOA. Thus, the measurement equation (1) is an integral relationship which is solved for M in terms of m. With a finite number of measurements, we can only define M in terms of space and time averages. Normally, the measurement equation is solved for the average regional or zonal radiant exitance for a day or month. The time averaging has been defined in the past by averaging all measurements that viewed a specific region at different times. This time average is biased, however, by the satellite sampling. A better approach is to form an instantaneous estimate of M and average over the length of a day with a diurnal directional function to determine the daily average exitance. This is the proposed approach for ERBE and necessitates an instantaneous estimate of the radiant exitance.

One way to form an instantaneous estimate of M is to determine the shape factor between the radiation field and the measurement. Let us assume that the radiation field is measured at $t_{i+1} = t_i + \Delta t$, $i = 1, 2, \cdots$ and that M is constant over the FOV. Also, if R is independent of latitude and longitude, then the measurement equation (1) can be written at time t_i as

$$m_i = M_i \pi^{-1} \int_{\text{FOV}} R(\theta) \cos\alpha d\Omega,$$

which reduces to

$$\hat{M}_i = \left(\frac{r+h}{r}\right)^2 m_i, \quad (2)$$

where the circumflex ($\hat{}$) denotes estimate. This is the familiar inverse square law where r is the Earth's radius to the TOA.

The wide angle measurement as defined in (1) smooths the spatial variation. Eq. (2) adjusts the magnitude of the measurement to correspond to the TOA but does not enhance or unsmooth the radiation field. A technique that does enhance the estimates along the groundtrack of the satellite is given by the numerical filter

$$\hat{M}_i = \sum_{j=-n}^{n} \omega_j m_{i+j}, \quad (3)$$

where the estimate of the radiant exitance at nadir is obtained by summing over a sequence of $2n + 1$ measurements, and where ω_j are the inversion weights chosen in an optimum way. We refer to (3) as an N point, one-dimensional numerical filter that enhances the estimate where $N = 2n + 1$.

There are a number of different ways to define the inversion weights. We will consider a matrix formulation. House and Jafolla (1980) defined the inversion weights with Fourier transforms. Basic to the one-dimensional numerical filter is the assumption that M is constant perpendicular to the groundtrack (see Fig. 1). Moreover, assume M constant within a strip perpendicular to the groundtrack and write (1) as

$$m_i = \sum_{j=-J}^{J} \hat{M}_{i+j} \pi^{-1} \int_{\text{FOV}_j} R(\Theta, \Phi, \theta) \cos\alpha d\Omega,$$

where J depends on how many strips are in the total FOV. Thus, we write

$$m_i = \sum_{j=-J}^{J} \gamma_j \hat{M}_{i+j}, \quad (4)$$

where the quadrature weights γ_j are given by

$$\gamma_j = \pi^{-1} \int_{\text{FOV}_j} R(\Theta, \Phi, \theta) \cos\alpha d\Omega. \quad (5)$$

Thus, from (4) we have one equation and $2J + 1$ unknown M_i's. If we consider a $2n + 1$ sequence of measurements and assume R independent of position so that the γ_j's are shift invariant, then the system of equations is given by

$$\begin{bmatrix} m_{i-n} \\ \vdots \\ m_i \\ \vdots \\ m_{i+n} \end{bmatrix} = \begin{bmatrix} \gamma_{-J} \cdots \gamma_0 \cdots \gamma_J & & \\ & \ddots & \\ & \gamma_{-J} \cdots \gamma_0 \cdots \gamma_J & \\ & & \ddots \\ & & \gamma_{-J} \cdots \gamma_0 \cdots \gamma_J \end{bmatrix} \begin{bmatrix} \hat{M}_{i-n-J} \\ \vdots \\ \hat{M}_i \\ \vdots \\ \hat{M}_{i+n+J} \end{bmatrix}, \quad (6)$$

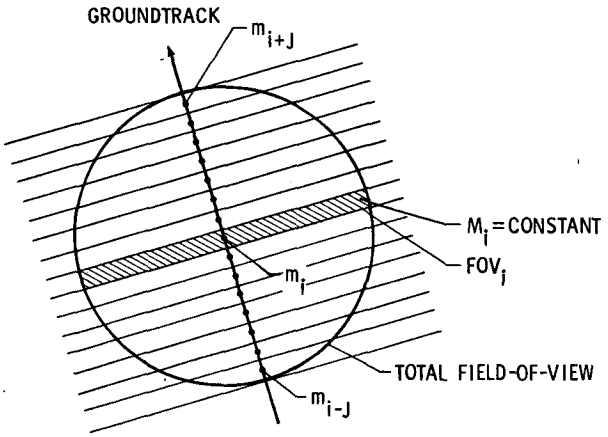

FIG. 1. Spatial geometry.

or $\mathbf{m} = \mathbf{B}\hat{\mathbf{M}}$ in matrix notation where $\mathbf{B}$ is a banded matrix. However, we still have an underdetermined system of equations with $2n + 1$ known measurements and $2n + 2J + 1$ unknown radiant exitances. To overcome this problem, we can assume that M is constant or persistent at both ends of the measurement sequence; that is, $M_{i\pm n} = M_{i\pm(n+1)} = \cdots = M_{i\pm(n+J)}$ which reduces $\mathbf{B}$ to a $(2n + 1)$ dimensional square matrix given by

$$\mathbf{B} = \begin{bmatrix} \sum_{i=-J}^{0} \gamma_i \cdots \gamma_J & & & \\ & \ddots & & \\ & & \gamma_{-J} \cdots \gamma_0 \cdots \gamma_J & \\ & & & \ddots \gamma_{-J} \cdots \sum_{i=0}^{J} \gamma_i \end{bmatrix}, \tag{7}$$

and the estimate of radiant exitance is

$$\hat{\mathbf{M}} = \mathbf{B}^{-1}\mathbf{m}.$$

The assumption of persistent M at the boundaries produces errors in the $\hat{M}_i$'s. It is fortunate that the least affected estimate is $\hat{M}_i$ since it is the center estimate and the most removed from the assumption. Finally, the inversion weights ω_j to estimate $\hat{M}_i$ are given by the center row of the $\mathbf{B}^{-1}$ matrix.

3. Error analysis

Let us define as "truth" a time independent, longwave radiant exitant field at the TOA as

$$M^*(\Theta, \Phi) = \sum_{n=0}^{N} \sum_{m=-n}^{n} C_n^m Y_n^m(\Theta, \Phi) \tag{8}$$

where Y_n^m are surface spherical harmonics and C_n^m are the Fourier coefficients. The asterisk denotes that M^* is the true radiant exitance. Synthetic measurements are easily determined from this representation of the radiation field by taking advantage of the nature of the measurement equation (1). Smith and Green (1981) have shown that spherical harmonics are the eigenfunctions of this integral equation so that

$$m^*(\Theta_s, \Phi_s, h; t) = \pi^{-1} \int_{\text{FOV}} \sum_{n=0}^{N} \sum_{m=-n}^{n} C_n^m Y_n^m(\Theta, \Phi) \times R(\theta) \cos\alpha \, d\Omega = \sum_{n=0}^{N} \sum_{m=-n}^{n} \lambda_n C_n^m Y_n^m(\Theta_s, \Phi_s), \tag{9}$$

where λ_n are the eigenvalues. The synthetic measurements become $m_i = m_i^* + \epsilon_i$, where ϵ_i is a random measurement error such that $E[\epsilon_i] = 0$ and $E[\epsilon_i \epsilon_j] = \sigma^2 \delta_{ij}$.

The residual error is defined as the difference between the estimated and true radiant exitance, that is

$$r_i \equiv \hat{M}_i - M_i^*$$

$$r_i = \sum_{j=-n}^{n} \omega_j (m_{i+j}^* + \epsilon_{i+j}) - M_i^*.$$

The expected value of the residual error is

$$E[r_i] = \sum_{j=-n}^{n} \omega_j m_{i+j}^* - M_i^* \equiv b_i,$$

which, in general, is not zero and is defined as a bias error b_i. This bias error represents the error introduced by the assumed spatial model; i.e., M is constant over FOV_j (see Fig. 1) and M is persistent at the boundaries. Also, we have

$$E[r_i^2] = E[(\hat{M}_i - M_i^*)^2] = b_i^2 + \sigma^2 \sum_{j=-n}^{n} \omega_j^2, \tag{10}$$

so that the variance of the residual error is

$$\text{Var}[r_i] = E[r_i^2] - E^2[r_i] = \sigma^2 \sum_{j=-n}^{n} \omega_j^2.$$

Now let us examine a set of K bias errors along the groundtrack. The rms bias error is given by

$$\text{rms}(b) = \left[\frac{1}{K} \sum_{k=1}^{K} b_k^2\right]^{1/2}. \tag{11}$$

The mean-squared residual error is

$$\text{ms}(r) = \frac{1}{K} \sum_{k=1}^{K} r_k^2,$$

and its expected value is

$$E[\text{ms}(r)] = \frac{1}{K} \sum_{k=1}^{K} E[r_k^2],$$

and from (10) and (11)

$$E[\text{ms}(r)] = \text{rms}^2(b) + \sigma^2 \sum_{j=-n}^{n} \omega_j^2.$$

We shall define the rms residual error as the square root of the expected mean-squared residual error; that is,

$$\text{rms}(r) = [\text{rms}^2(b) + \sigma^2 \sum_{j=-n}^{n} \omega_j^2]^{1/2}. \quad (12)$$

Notice that the rms residual error is composed of two terms. The first term is the rms bias error which is independent of the random measurement error, and the second term is the mean variance from the enhancement of the random measurement error which is dependent on the sum of the squared inversion weights. There is a relationship between the rms bias error and the magnitude of the inversion weights which dictates the rms residual error. Our objective is to determine the inversion weights that minimize these residual errors.

4. Simulation of numerical filter

The accuracy of the numerical filter estimate is best studied by simulating the data gathering and measurement inversion process. The number of measurements N that are processed together can also be studied with computer simulation.

Let us assume that the true radiation field at TOA can be represented by a 24 degree expansion in spherical harmonics where the Fourier coefficients are derived from Nimbus 6 data and the parameter estimation technique (Green, 1981). A contour plot of this radiation field and the groundtrack for one orbital revolution are shown in Fig. 2. The satellite is assumed to be in a circular orbit 833 km above the Earth's surface. Assuming the Earth's radius to be 6378 km, and defining the TOA at 30 km above, at a radius of $r = 6408$ km, then h is 803 km. The orbital period is approximately 102 min. For the purpose of simulation, synthetic measurements were generated every minute and the radiant exitance was estimated every minute for one full orbital revolution so that $K = 102$. It was also assumed that the angular directional model is Lambertian; i.e., $R(\Theta, \Phi, \theta) = 1$. The true measurements m_i^*, as defined in (9) for the assumed geometry, are presented in Fig. 3. The quadrature weights γ_j as defined in (5) are presented in Fig. 4. The quadrature weights for this case are symmetric about the nadir since the angular directional model is independent of latitude and longitude. A measurement sampling rate of 1 min defines the strips of constant M perpendicular to the groundtrack (Fig. 1) as 3.5° wide; and, since the diameter of the FOV is 54.6°, we have that γ_0 is the integral over an area of approximately 400 × 6100 km. Also note that the sum of the quadrature weights represents the integration over the entire FOV such that from (2)

$$\sum_{j=-8}^{8} \gamma_j = \left(\frac{r}{r+h}\right)^2.$$

With these quadrature weights, we form the $\mathbf{B}$ matrix (7) and set the inversion weights ω_j equal to the center row of $\mathbf{B}^{-1}$. For example, a 9 point numerical filter yields $\omega_0 = 27.48$, $\omega_{\pm 1} = -20.08$, $\omega_{\pm 2} = 10.13$, $\omega_{\pm 3} = -4.17$, and $\omega_{\pm 4} = 1.01$. These weights are used to estimate $\hat{M}_i$.

Let us examine the rms bias errors for one orbital revolution. Different length numerical filters give different rms bias errors. A plot of these errors versus the number of points N in the filter is given in Fig. 5. The top curve was generated with inversion weights derived from $\mathbf{B}^{-1}$ and show that as N increases, the rms bias error decreases and asymptotically approaches a value of ~4 W m^{-2}. These rms bias errors result from the spatial assumptions and cannot be reduced further with the numerical filter where the

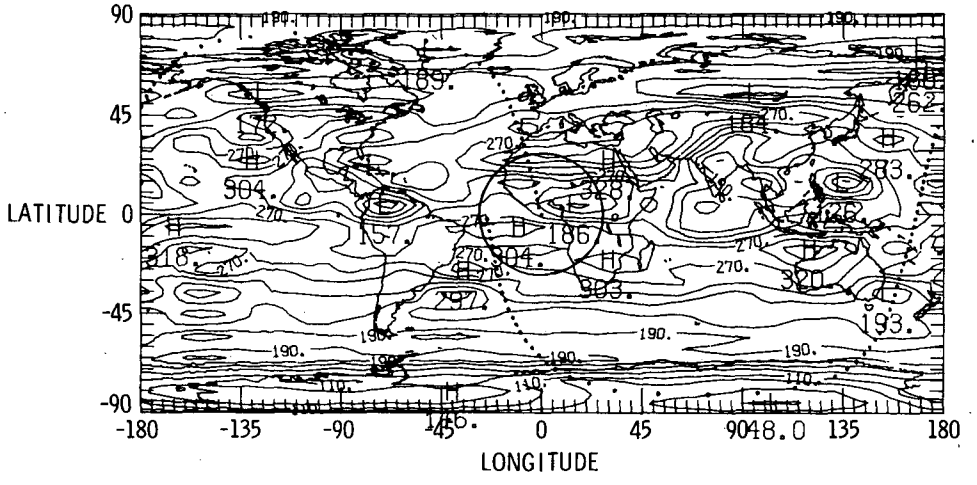

FIG. 2. True longwave radiation field and measurement points.

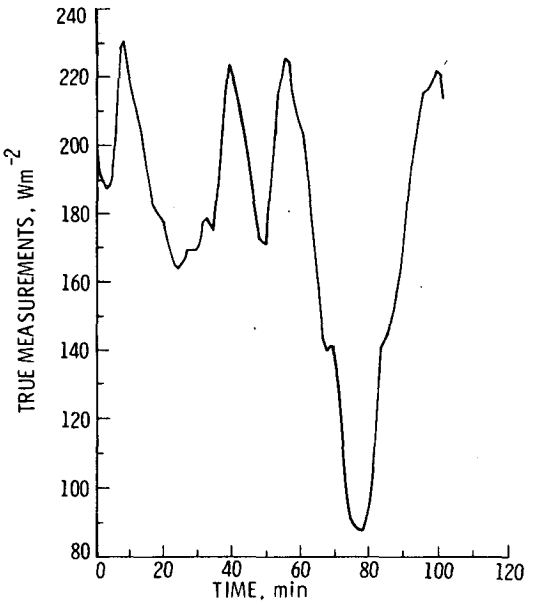

FIG. 3. One hundred and two true measurements.

inversion weights are derived from $\mathbf{B}^{-1}$. It is reassuring, however, that the 102 bias errors summed to approximately zero for all cases. An absolute minimum rms bias error can be established by deriving the ω_i's that minimize rms(b). These optimum weights are given in vector form as

$$\omega_{\text{opt}} = (\mathbf{m}^{*T}\mathbf{m}^{*})^{-1}\mathbf{m}^{*T}\mathbf{M}^{*},$$

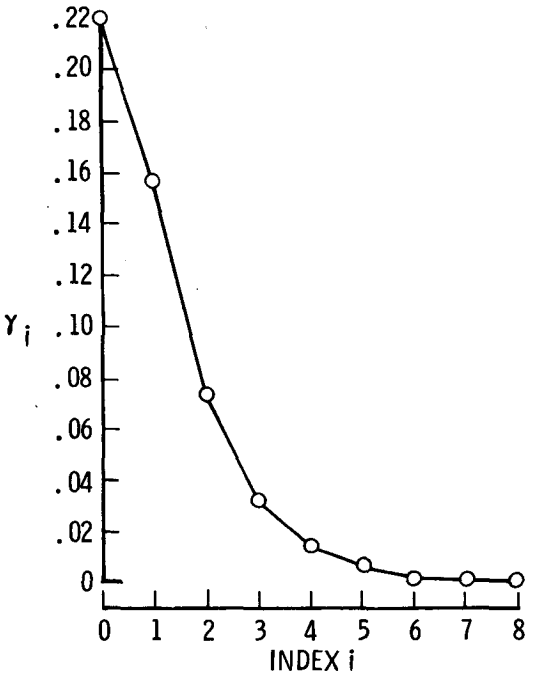

FIG. 4. Quadrature weights γ_i.

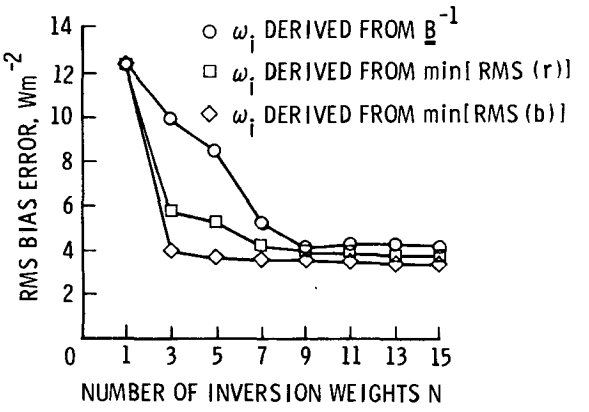

FIG. 5. Bias errors.

where $\mathbf{m}^*$ is a 102 by N matrix of measurements

$$\mathbf{m}^* = \begin{bmatrix} m^*_{1-n} & \cdots & m^*_1 & \cdots & m^*_{1+n} \\ m^*_{2-n} & \cdots & m^*_2 & \cdots & m^*_{2+n} \\ \vdots & & \vdots & & \vdots \\ m^*_{102-n} & \cdots & m^*_{102} & \cdots & m^*_{102+n} \end{bmatrix}$$

and $\mathbf{M}^*$ is a column vector of the 102 true radiant exitances. These optimum weights are a function of the true field and represent an unobtainable solution. They do, however, establish a lower bound on the rms bias error. The minimum rms bias errors corresponding to these ω_{opt} are given in Fig. 5 and asymptotically decrease to $\sim$3.2 W m^{-2}. Thus, the inversion weights based on $\mathbf{B}^{-1}$ give rms bias errors which are close to the optimum results.

If the measurements were error free, then a good solution of the inversion problem would be a 9-point numerical filter since increasing N beyond 9 gives little improvement. However, from (12) we know that the rms residual error is a function not only of the bias errors, but also a function of the magnitude of the inversion weights. For the 9-point numerical filter being considered, this magnitude is $\sum_{j=-4}^{4} \omega_j^2 = 1803.67$. Assuming a 1 W m^{-2} standard deviation error of the measurement results in an rms(r) = $[(4.05)^2 + 1803.67]^{1/2}$ = 42.66 W m^{-2}. Obviously, this magnitude of error is unacceptable. Even the optimum inversion weights have a magnitude of 82.93 and an rms bias error of 3.49 W m^{-2} such that rms(r) = $[(3.49)^2 + 82.93]^{1/2}$ = 9.75 W m^{-2} which is also a large error.

Let us determine a set of optimum inversion weights that will minimize rms(r) or simultaneously minimize both the bias errors and the magnitude of the inversion weights. This set of inversion weights is given by

$$\omega_{\text{opt}} = (\mathbf{m}^{*T}\mathbf{m}^{*} + K\sigma^2\mathbf{I})^{-1}\mathbf{m}^{*T}\mathbf{M}^{*}. \qquad (13)$$

These optimum weights do not represent a solution since they are based on the true radiation field, but they do represent the limit of what could be achieved. The rms bias errors corresponding to these optimum weights are also presented in Fig. 5. We observe that these rms bias errors increased only a small amount as a result of reducing the magnitude of the inversion weights. Specifically, for a 9 point numerical filter, the magnitude of weights was 9.76, and the rms bias error was 3.91 W m^{-2} which resulted in an rms(r) = $[(3.91)^2 + 9.76]^{1/2}$ = 5.00 W m^{-2}. This shows that the magnitude of the weights can be reduced significantly with very little penalty in the rms bias errors. Actually, the rms bias error was increased from 3.49 W m^{-2} to 3.91 W m^{-2} above its lower limit for a reduction in the rms residual error of from 9.75 W m^{-2} to 5.00 W m^{-2}. The conclusion is that inversion weights do exist that not only give small bias errors, but also have small magnitudes so that they are not highly sensitive to measurement error. It remains to determine a method to calculate some near optimum inversion weights.

5. Smoothed numerical filter

The system of simultaneous equations that defines the inversion weights is given by (6) and (7) as

$$\mathbf{m} = \mathbf{B}\hat{\mathbf{M}},$$

or

$$\mathbf{m} = \mathbf{U}\mathbf{Q}\mathbf{V}^T\hat{\mathbf{M}}, \tag{14}$$

where the columns of $\mathbf{U}$ and $\mathbf{V}$ are the left and right singular vectors of $\mathbf{B}$, respectively, and $\mathbf{Q}$ is a diagonal matrix containing the nonnegative singular values (Forsythe *et al.*, 1977). This singular value decomposition of $\mathbf{B}$ yields the solution

$$\hat{\mathbf{M}} = \mathbf{V}\mathbf{Q}^+\mathbf{U}^T\mathbf{m},$$

where $\mathbf{Q}^+$ is the pseudo inverse of $\mathbf{Q}$. If the singular values and their corresponding singular vectors are ordered from largest to smallest, then examination of $\mathbf{V}$ reveals that the first singular vector is an array of almost constant elements and corresponds to a singular value of 0.8016 for a 9-point numerical filter. The last singular vector is characterized by elements of alternating sign and has a singular value of 0.0121. The reciprocals of the singular values which compose $\mathbf{Q}^+$ show that the alternating pattern of signs in the last singular vector will be much more prominent in the solution than the constant pattern of the first singular vector. It follows that the solution can be "smoothed" by setting the smallest singular value in $\mathbf{Q}$ equal to zero and taking the center row of $\mathbf{V}\mathbf{Q}^+\mathbf{U}^T$ as the inversion weights. To conserve energy, however, these smoothed weights must be normalized such that

$$\sum_{i=-n}^{n} \omega_i = \left(\frac{r+h}{r}\right)^2.$$

The justification for arbitrarily setting the smallest singular value to zero is an approximation theorem which states that the distance from the matrix $\mathbf{B}$ to the closest matrix of rank $N-1$ is the Nth largest singular value. Furthermore, this matrix is obtained by setting the Nth singular value to zero in the decomposition $\mathbf{B} = \mathbf{U}\mathbf{Q}\mathbf{V}^T$. Thus, by setting the smallest singular value to zero, we closely approximate the simultaneous system of equations (7) while smoothing the solution. Additional smoothing is obtained by setting the other singular values to zero from smallest to largest.

The various sets of smoothed inversion weights for a 9-point numerical filter are given in Table 1. If all nine singular values are retained in the solution, we see that the magnitude of the weights is large and that

TABLE 1. Various solutions for a 9-point numerical filter.

Solution characteristics	Number of singular values* in solution					Optimum solutions	
	9	8 or 7	6 or 5	4 or 3	2 or 1	rms(b)	rms(r)
ω_{-4}	1.01	−1.35	0.74	−0.27	0.26	−0.20	0.43
ω_{-3}	−4.17	4.00	−1.07	−0.03	0.14	1.70	−0.58
ω_{-2}	10.13	−4.22	−1.03	0.24	0.13	−4.65	−1.08
ω_{-1}	−20.08	−1.36	0.92	0.44	0.13	4.18	0.76
ω_0	27.48	7.13	2.13	0.51	0.13	−0.78	2.19
ω_1						4.18	0.84
ω_2			Symmetric about ω_0			−4.55	−1.11
ω_3						1.45	−0.71
ω_4						−0.07	0.52
$\Sigma\ \omega_i$	1.26	1.26	1.26	1.26	1.26	1.27	1.27
$\Sigma\ \omega_i^2$	1803.67	125.80	11.73	0.91	0.18	82.93	9.76
mean b_i	0.02	0.01	0.02	0.11	0.15	0.24	0.28
rms(b)	4.05	5.74	4.07	11.65	20.84	3.49	3.91
rms(r)	42.66	12.60	5.32	11.70	20.85	9.75	5.00

* Singular values: 0.8016, 0.7022, 0.4722, 0.2755, 0.1555, 0.0837, 0.0434, 0.0222, 0.0121.

they alternate in sign. The center weight is 27.48. Solving for the weights with either seven or eight singular values gives the same solution where the center weight is reduced to 7.13. This set of weights is smoother and reduces the rms residual error from 42.66 to 12.60 W m^{-2}. The solution with the lowest rms(r) is determined with five or six singular values. Decreasing the number of singular values beyond this point reduced

$$\sum \omega_i^2,$$

but at the expense of increasing the bias errors due to the lack of enhancement. Thus, for a 9-point numerical filter, the best smoothed solution corresponds to retaining five or six singular values. Fig. 6 shows the rms residual error for the best smoothed solutions as a function of N, the number of points in the filter. Again, a 9-point smoothed numerical filter would be a good choice since it minimizes rms(r).

The alternation of local maxima and minima in Fig. 6 is possibly the result of the discrete smoothing. For example, by setting the singular values to zero in the 9-point numerical filter, we only produced four different smoothed solutions. The 3-point numerical filter only had one smoothed solution which introduced too much smoothing resulting in the local maximum. Other methods that continuously apply the smoothing would probably not result in the alternation of local maxima and minima seen in Fig. 6.

6. Resolution

Throughout this study, we have compared the estimates at the TOA with the true radiation field evaluated at the nadir point. These estimates, however, are more representative of the average radiant exitance over an area than they are of a single point. Thus, let us define the area of a spherical cap with radius θ about the nadir point and determine the average radiant exitance $\bar{M}^*$ over this area. We also define the residual as a function of θ or

$$r_i(\theta) = \hat{M}_i - \bar{M}_i^*(\theta).$$

The estimates will be most representative of the area defined by the θ that minimizes the rms residual error or rms[$r(\theta)$].

In terms of the spherical radius θ and the azimuth ξ about nadir, the average radiant exitance is

$$\bar{M}^*(\Theta_s, \Phi_s, \theta) = \frac{\int_0^{2\pi}\int_0^{\theta} M^*(\Theta, \Phi)\sin\theta d\theta d\xi}{\int_0^{2\pi}\int_0^{\theta}\sin\theta d\theta d\xi}. \quad (15)$$

If M^* is represented by a spherical harmonic expansion, then (15) and (8) reduce to

$$\bar{M}_i^*(\theta) = \sum_{n=0}^{24}\sum_{m=-n}^{n} \beta_n(\theta) C_n^m Y_n^m(\Theta_i, \Phi_i),$$

where $\beta_n(\theta)$ is the Pellinen smoothing parameter (Pellinen, 1966) given by

$$\beta_n(\theta) = \frac{1}{1-\cos\theta}\int_0^{\theta} P_n(\cos\theta)\sin\theta d\theta.$$

The smoothing parameter is presented in Fig. 7 for various size circular areas. Naturally, the larger the averaging area, the more the high frequency spatial components of the spherical harmonic representation will be attenuated by the decreasing β_n's.

We can now compare the estimates $\hat{M}_i$ with the radiant exitance over a spherical cap $\bar{M}_i^*$. Fig. 8 presents the relationship between accuracy and resolution for various numerical filters. For example, the

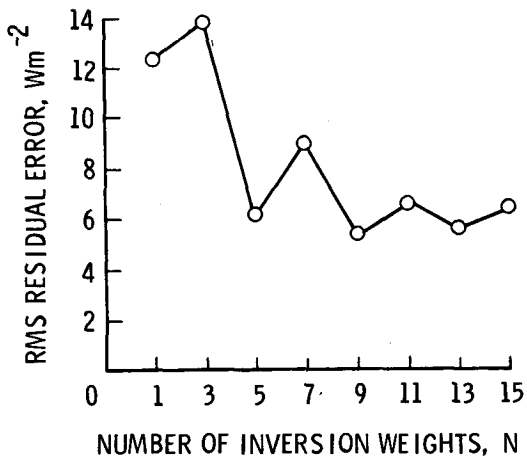

FIG. 6. Residual errors for best smoothed numerical filter.

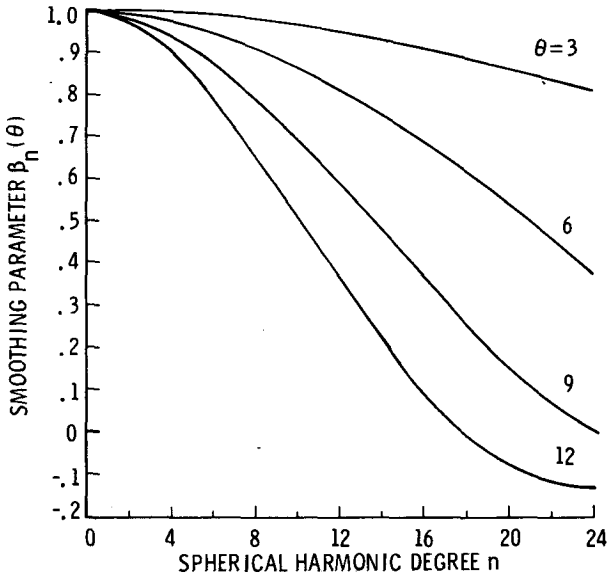

FIG. 7. Spherical cap smoothing parameter.

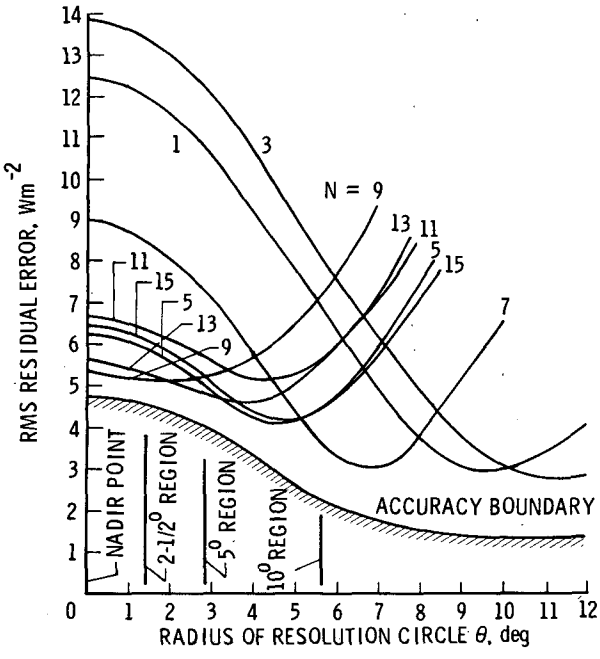

FIG. 8. Accuracy and resolution for best smoother numerical filter.

numerical filter which best represented the radiant exitance at nadir ($\theta = 0°$) was determined from Fig. 6 as the smoothed 9-point filter where the rms residual error (accuracy) was 5.32 W m^{-2}. From Fig. 8, we see that the rms residual error is slightly reduced with increasing θ (resolution) reaching a minimum at $\sim\theta = 2°$. As θ increases beyond this value, the errors also increase. This implies that a set of inversion weights that enhance the measurements produce estimates that correspond to small areas and not large areas. Thus, a smoothed 9-point numerical filter best represents the average radiant exitance in a spherical cap of radius 2°. At a resolution of 2°, however, a 13-point smoothed numerical filter is slightly more accurate than the 9-point filter. At a 4° resolution, a 5-point filter performs best, and at a 7° resolution, a 7-point filter is best. The 1-point numerical filter in this study is equivalent to the inverse square law (2), and is seen to give inaccurate estimates for a small area. However, it has a minimum at $\theta = 10°$, and accurately estimates the average radiant exitance over that area with an rms residual error of 3.01 W m^{-2}. This area produces ~75% of the measurement. The half power area corresponds to $\theta = 6°$. It is clear that no one numerical filter is best for all resolutions and that the inversion weights should be determined on the basis of the desired resolution. Many times the desired resolution is expressed in terms of square regions instead of circular regions. The radius of resolution θ that corresponds on an equal area basis to a square region is also shown in Fig. 8. If we want to estimate the 5 × 5° regional radiant exitance, then a smoothed 13-point numerical filter would be best where the inversion weights are based on the eight largest singular values of the measurement matrix.

There is a bound to the accuracy that can be expected from a numerical filter. A set of inversion weights that minimize rms(r) are given by (13). These weights correspond to $\theta = 0°$. It is straightforward to determine another set of optimum inversion weights that minimize rms[$r(\theta)$] by replacing $\bar{M}^*$ with $\bar{M}^*(\theta)$. The optimum weights establish a lower bound on the accuracy which is presented in Fig. 8 as a function of θ. This curve was actually computed with a 15-point numerical filter which has enough degrees of freedom to represent the bounding condition. We see that the smoothed inversion weights defined with the matrix formulation and persistent boundary assumption and solved with the singular value decomposition are very near optimum.

7. Summary and conclusions

We have seen that the residual error between the estimated radiant exitance and true radiant exitance is composed of two different errors. The first is a bias error which results from the spatial assumption necessary to reduce a two-dimensional estimation problem to a one-dimensional problem. The second error is of a random nature and results from random measurement error.

The expected value of each estimate of radiant exitance at the TOA is biased. This bias error depends on the true radiation field and the latitude and longitude of the estimate. It is difficult to define the nature of this bias for a particular latitude and longitude since we do not know the ensemble of radiation fields that can occur at that point. However, we can simulate the bias at different points for one typical radiation field. Synthetic measurements were generated every minute along a typical satellite orbit, and the radiation field was estimated at 102 points along the groundtrack for one complete orbital revolution. It was found that the average of the 102 biases was near zero. This implies that the average radiant exitance over large areas can be estimated with little bias by averaging individual estimates. The rms value for these bias errors depends on the numerical filter selected and on the resolution area to which the estimate is compared. For example, if we desire to estimate the radiant exitance averaged over a 5 × 5° region, then a smoothed 13-point numerical filter is best. The rms bias error for this case was 3.67 W m^{-2}. This bias error can be compared to an rms bias error of 2.67 W m^{-2} which was determined by minimizing the rms bias error knowing the "true" field. It can also be compared to an rms bias error of 2.96 W m^{-2} which was determined by minimizing the rms residual error knowing the true field. Obviously, these minimum bias errors are unobtainable, but represent the lower boundary of the error. Another way to in-

terpret these findings is to consider the rms as a measure of standard deviation since the average of the biases is near zero. In addition, if we interpret this variance over space to represent the ensemble variation at one latitude and longitude (Ergodic Assumption), then we can make statistical statements about the accuracy of the estimates. Moreover, if we venture to think of the biases as being normally distributed, then we can associate a confidence to these findings. Thus, in the absence of angular directional model errors and for error-free measurements, we can be 90% confident that the radiant exitance averaged over a $5 \times 5°$ region can be estimated to within ± 6.03 W m^{-2}. To be 99% confident, we must extend the confidence interval to ± 9.45 W m^{-2}.

The second error source that contributes to the residual error is the measurement error. As discussed above, the expected value of a residual error is a bias and is not affected by measurement errors. However, the statistical variance of each residual error is $\sigma^2 \sum_{i=-n}^{n} \omega_i^2$ where σ is the standard deviation of the measurement error. Whereas the bias was position and space dependent, the variance is independent of both. This means that we can make a general statement about the variance of the residual error. For example, if the measurement error is approximately 0.5% ($\sigma = 1$ W m^{-2}) and a 13-point smoothed numerical filter is applied to the measurements, then the variance of the residual error is 9.84 W^2 m^{-4} which gives a standard deviation of 3.14 W m^{-2}. When the variation due to the measurement error is added to the variation due to the bias error, the confidence interval of the estimate is increased. Thus, in the absence of angular directional model errors and with measurement errors defined by $\sigma = 1$ W m^{-2}, we are 90% confident that the average radiant exitance over a $5 \times 5°$ region can be estimated to within ± 7.94 W m^{-2}, and 99% confident that it will be between ± 12.43 W m^{-2}.

These confidence intervals were tested by simulating the estimation process over the entire globe. Eight orbital revolutions were considered with the ascending nodes increased by 24° for each revolution. Synthetic measurements were generated by adding random errors from a random number generator to the true measurements. Finally, the radiation field was estimated with the numerical filter and compared to the true field. This simulation generated 816 random residual errors over the globe. From Fig. 8, we would expect the rms residual error to be 4.83 W m^{-2}. The test results are based on the actual random measurement errors and gave a value of 4.64 W m^{-2}. We would expect 90% or 734 residuals to be within ± 7.94 W m^{-2}. The test results gave 742 residuals within this range. We would expect only 1% or eight of the residuals to be outside the range ± 12.43 W m^{-2}. The test results gave 13 residuals outside this range. Thus, we conclude that the assumptions made to determine confidence intervals are valid based on these test results. We also conclude that the numerical filter performs well over the entire globe even though its design was based on the measurements from a single orbital revolution.

REFERENCES

Bess, T. D., R. N. Green and G. L. Smith, 1981: Deconvolution of wide field-of-view radiometer measurements of Earth-emitted radiation. Part II: Analysis of first year of Nimbus 6 ERB wide angle Earth-emitted data. *J. Atmos. Sci.*, **38,** 474–488.

Forsythe, G. E., M. A. Malcolm and C. B. Moler, 1977: *Computer Methods for Mathematical Computations.* Prentice–Hall, 255 pp.

Green, R. N., 1980: The effect of directional radiation models on the interpretation of Earth radiation budget measurements. *J. Atmos. Sci.*, **37,** 2298–2313.

——, 1981: The effect of data analysis techniques on the interpretation of wide-angle longwave radiation measurements. *J. Atmos. Sci.*, **38,** 2045–2055.

House, F. B., and J. C. Jafolla, 1980: One dimensional technique for enhancing Earth radiation budget observations from Nimbus 7 Satellite. Presented at 1980 Int. Radiation Symp., Fort Collins, 392–394.

King, M. D., and R. J. Curran, 1980: The effect of a nonuniform planetary albedo on the interpretation of earth radiation budget observations. *J. Atmos. Sci.*, **37,** 1262–1278.

Pellinen, L. P., 1966: A method for expanding the gravity potential of the earth in spherical functions. *Trans. Central Scientific Research Institute of Geodesy, Aerial Survey and Cartography.* Issue 171, 92 pp., [NTIS Transl. ACIC-TC01282].

Smith, G. L., and R. N. Green, 1981: Deconvolution of wide field-of-view radiometer measurements of Earth emitted radiation. Part I: Theory. *J. Atmos. Sci.*, **38,** 461–473.

Weaver, W. L., and R. N. Green, 1980: Simulation study of geometric shape factor approach to estimating Earth emitted flux densities from wide field-of-view radiation measurements. *Remote Sens. Environ.*, **9,** 265–276.